Unveiling galaxy chemical enrichment mechanisms out to cosmic dawn from direct determination of O Ar abundances from JWST/NIRSPEC spectroscopy

Souradeep Bhattacharya  $^{\hbox{\scriptsize 1}}$   $^2$  Magda Arnaboldi  $^{\hbox{\scriptsize 1}}$   $^3$  Ortwin Gerhard  $^{\hbox{\scriptsize 1}}$   $^4$  Chiaki Kobayashi  $^{\hbox{\scriptsize 1}}$   $^2$  and Kanak Saha  $^{\hbox{\scriptsize 1}}$ 

Inter-University Centre for Astronomy and Astrophysics, Ganeshkhind, Post Bag 4, Pune 411007, India

<sup>2</sup> Centre for Astrophysics Research, Department of Physics, Astronomy and Mathematics, University of Hertfordshire, Hat eld, AL10

9AB, UK

<sup>3</sup>European Southern Observatory, Karl-Schwarzschild-Str. 2, 85748 Garching, Germany
<sup>4</sup>Max-Planck-Institut f
ür extraterrestrische Physik, Giessenbachstraße, 85748 Garching, Germany

(Received August 27, 2024)

Submitted to ApJL

#### ABSTRACT

Galaxy chemical enrichment mechanisms have primarily been constrained by [ /Fe] and [Fe/H] measurements of individual stars and integrated light from stellar populations. However such measurements are limited at higher redshifts (z>1). Recently, we proposed an analogous diagram of the oxygen-to-argon abundance ratio,  $\log(\mathrm{O/Ar})$ , vs Ar abundance,  $12+\log(\mathrm{Ar/H})$ , as a new diagnostic window for emission nebulae. In this Letter, using robust line flux measurements including temperature sensitive auroral lines, we present direct determination of O and Ar abundances in nine SFGs from JWST/NIRSPEC spectra at  $z\sim1.3-7.7$ , and two more with Keck/MOSFIRE spectra at  $z\sim2.2$ . Utilising their positions on the  $\log(\mathrm{O/Ar})$  vs  $12+\log(\mathrm{Ar/H})$  plane, we present the first inference of galaxy chemical enrichment mechanisms from an ensemble of galaxies. The SFGs at  $z\sim1.3-3.4$  are consistent with the solar neighbourhood galactic chemical enrichment models of the Milky Way Galaxy that are driven by core-collapse and Type Ia supernovae. Such enrichment mechanisms thus occur at least out to  $z\sim3.4$ . However, the highest-redshift SFGs ( $z\sim3.6-7.7$ ) have very low  $\log(\mathrm{O/Ar})$  values, revealing a di erent enrichment process at z>3.6. Such low  $\log(\mathrm{O/Ar})$  values may be caused by a rapid but intermittent star-formation and/or additional sources. The new diagnostic window for SFGs enables us to reveal the unique fingerprints of galaxy chemical enrichment out to cosmic dawn.

Keywords: Chemical abundances (224); Galaxy formation (595); Galaxy chemical evolution (580); James Webb Space Telescope (2291); Supernovae (1668); Milky Way Galaxy (1054)

## 1. INTRODUCTION

Since the break of cosmic dawn, the interstellar medium (ISM) of galaxies has been continually enriched by the birth and death of stars. The bulk of our understanding of galaxy chemical enrichment (Tinsley 1980; Pagel 1997; Kobayashi et al. 2020a; Matteucci 2021) stems from spectroscopic observations of individual stars in our Milky Way (MW) and studies of nearby galax-

Corresponding author: Souradeep Bhattacharya souradeep@iucaa.in, s.bhattacharya3@herts.ac.uk

ies. Deep absorption line spectra of MW stars enabled determination of their [Fe/H] and [ /Fe], revealing the chemical composition of the ISM at the time of their birth (e.g. Edvardsson et al. 1993; Fuhrmann 1998; Hayden et al. 2015). The stars showing the highest [ /Fe] values are thought to have formed at the earliest times from ISM that had only been enriched by core-collapse (CCSNe). Once Type Ia supernovae (SNe Ia) explosions begin, more Fe is released to the ISM than previously, causing a decreasing trend in [ /Fe] vs [Fe/H] for the subsequent generations of stars.

To constrain early chemical enrichment mechanisms, [ /Fe] and [Fe/H] measurements of the oldest genera-

tions of stars are required. This is also possible from [ /Fe] and [Fe/H] determined from integrated stellar spectra of early-type galaxies (e.g. Trager et al. 2000; Thomas et al. 2005; Kuntschner et al. 2010; Greene et al. 2013). At high redshift ( $z\sim 2$ ), only a few quiescent massive galaxies have integrated stellar spectra with sufficiently deep absorption lines to enable determination of [ /Fe] and [Fe/H] (Lonoce et al. 2015; Onodera et al. 2015; Kriek et al. 2016; Beverage et al. 2024a,b). The vast majority of galaxies, however, are star-forming (SFGs) with their fraction increasing with increasing redshift. [Fe/H] can also be estimated from rest-frame UV continuum and combined to abundance from emission lines; [ /Fe] has been discussed for a few SFGs out to z~3.4 (e.g. Steidel et al. 2016; Cullen et al. 2019, 2021; Topping et al. 2020; Stanton et al. 2024).

Recently, the log(O/Ar) vs 12 + log(Ar/H) plane for emission nebulae was found to be analogous to the [ /Fe] vs [Fe/H] plane for stars (Arnaboldi et al. 2022). This was based on the analysis of emission-line spectra of planetary nebulae and HII regions surveyed in the Andromeda galaxy (M 31; Bhattacharya et al. 2019, 2021) where temperature sensitive auroral lines had been observed (Bhattacharya et al. 2022; Esteban et al. 2020). Like Fe, SNe Ia also preferentially produce more Ar than light -elements like O, whereas CCSNe produce nearconstant log(O/Ar), see Kobayashi et al. (2020a). Based on this concept, Arnaboldi et al. (2022) introduced the  $\log(O/Ar)$  vs  $12 + \log(Ar/H)$  plane using planetary nebulae to reveal the chemical enrichment history of M 31 with high star-formation at early times (> 8 Gyr ago) and gas-infall ~2-4 Gyr ago. Kobayashi et al. (2023) then showed that with well-constrained GCE models, the  $\log(O/Ar)$  vs  $12 + \log(Ar/H)$  plane can be connected to the [ /Fe]-[Fe/H] plane.

The spectra of SFGs are dominated by the emissionlines radiated by their constituent HII regions and diffuse ionised gas (Sargent 1970). Using abundance planes derived from their spectra such as  $\log(\mathrm{O/Ar})$  vs 12 +  $\log(\mathrm{Ar/H})$  thus opens up the possibility to constrain the chemical enrichment of SFGs.

With the advent of the NIRSPEC multi-slit spectroscopy instrument on board the James Webb Space Telescope (JWST; Jakobsen et al. 2022), direct elemental abundance determination has become possible for a number of SFGs out to  $z\sim 8.5$  (e.g. Curti et al. 2023; Nakajima et al. 2023; Sanders et al. 2024) through the detection of the temperature sensitive auroral [OIII] $\lambda$  4363 Å line. This allows the determination of abundances of a number of elements like O, Ne, S, Ar and N (e.g. Isobe et al. 2023).

These elemental abundances trace the state of the cumulative chemical enrichment of its ISM by previous generations of stars. As we move to higher redshifts, the chemical abundances in galaxies increasingly map the chemical enrichment from the very early generations of stars. As the relative contribution of CCSNe and SNeIa varies for the production of di erent elements (see Kobayashi et al. 2020a), we may use the relative abundances of di erent elements to decipher the state of chemical enrichment of each SFG at their observed redshift.

Rogers et al. (2024) and Welch et al. (2024) determined  $\log({\rm O/Ar})$  values for two SFGs at z~1.3 and z~3 respectively. Rogers et al. (2024) utilised the aforementioned results (Kobayashi et al. 2020a; Arnaboldi et al. 2022) to interpret the state of chemical enrichment of their individual SFG with a super-solar  $\log({\rm O/Ar})$  value as being primarily enriched by CCSNe. Individual SFGs may occupy di erent positions in the  $\log({\rm O/Ar})$  vs 12 +  $\log({\rm Ar/H})$  plane, and thereby exhibit di erent states of chemical enrichment. However, by determining the positions of an ensemble of high-z SFGs in this plane, we can constrain the mechanisms that drive early galaxy chemical enrichment.

In this work, we present the state of chemical enrichment in an ensemble of 11 SFGs at  $z\sim1.3$ –7.7 from their O & Ar abundances, providing constraints on the galaxy enrichment mechanisms at these redshifts. The data and determination of O & Ar abundances is presented in Section 2. The positions of these galaxies in the  $\log(O/Ar)$  vs  $12 + \log(Ar/H)$  plane and its implications for early galaxy chemical enrichment is discussed in Section 3. We conclude in Section 4.

## 2. DATA AND ABUNDANCE DETERMINATION

### 2.1. Galaxy sample

We build a sample of high-redshift (z>1) galaxies with O and Ar abundances determined directly via the detection of temperature sensitive auroral lines. For this purpose, we identify galaxies that have O abundances published already in the literature from their  $[OIII]\lambda$  4363 Å line detected in JWST/NIRSPEC observations.

We first searched for their publicly available flux and wavelength calibrated 1D JWST/NIRSPEC grating spectra and verified if their [OIII]  $\lambda$  4363 Å line was detected with with signal-to-noise S/N> 3 in these spectra. We then check if ionised Ar lines were also present (with S/N> 3). This procedure resulted in a sample of nine such galaxies for which we obtain direct determination of both O and Ar abundances. The flux determination procedure for these sources is laid out in Section 2.2. The [OIII]  $\lambda$  4363 Å and ionised Ar line fluxes

Table 1 Measurements of emission line fluxes for galaxies in this work from their flux and wavelength calibrated 1D JWST/NIRSPEC spectra.

Name	z	c(H\beta)		Line Flux (S/N)	x (S/N)		Source	Reference
			[OIII] 4363 Å	[OIII] 4363 Å [ArIV] 4711 Å [ArIV] 4740 Å [ArIII] 7136 Å	[ArIV] 4740 Å	[ArIII] 7136 Å	1D spectra	Line flux
ERO 10612	99.2	$0.38 \pm 0.15$	$23.76 \pm 2.48 (8.3)$	$10.81 \pm 2.87 \ (3.27)$ $10.39 \pm 2.54 \ (3.33)$	$10.39 \pm 2.54 (3.33)$	ı	$MAST^b$	Curti et al. (2023)
CEERS 1536	5.038	$0.95 \pm 0.06$	$31.9 \pm 7.53 (4.24)$	1	1	$31.38 \pm 7.9 \ (3.96)$	CEERS DR07 $^{c}$	Nakajima et al. (2023)
$GLASS 150029^a$	4.584		$0.25 \pm 0.03$ $17.34 \pm 2.71$ (6.64)	ı	ı	$11.03 \pm 3.1 \ (3.89)$	$MAST^b$	Nakajima et al. (2023)
CEERS $1665^a$	4.488	$0.4 \pm 0.03$	$6.53 \pm 1.98 \ (3.3)$	ı	1	$34.45 \pm 5.75 (8.54)$	CEERS DR07 $^{c}$	Sanders et al. (2024)
CEERS 1651	4.382	$0.89 \pm 0.1$	$12.36 \pm 0.04 \ (3.77)$	1	$38.97 \pm 4.13 \ (8.94)$	$18.21 \pm 3.65 \ (5.32)$	CEERS DR07 $^{c}$	Sanders et al. (2024)
GLASS 40066	4.02	$0.34 \pm 0.04$	$8.35 \pm 1.09 (4.71)$	1	1	$18.63 \pm 3.12 \ (4.95)$	$MAST^b$	Isobe et al. (2023)
JADES 19519	3.604	$0.07 \pm 0.02$	$24.54 \pm 7.36 (3.8)$	I	I	$4.23 \pm 1.39 \ (3.22)$	Bunker et al. (2023)	Morishita et al. (2024)
CEERS 11088	3.302	$0.72 \pm 0.07$	$5.74 \pm 1.98 \ (3.45)$	ı	ı	$24.07 \pm 4.57 (6.55)$	CEERS DR07 $^c$	Sanders et al. (2024)
CEERS 3788	2.295	$0.42 \pm 0.05$	$0.42 \pm 0.05$ $7.67 \pm 1.6$ (4.78)	1	ı	$16.33 \pm 2.68 \ (4.94)$	CEERS DR07 $^{c}$	Sanders et al. (2024)

NOTE—Column 1: Name of galaxy; Column 2: galaxy redshift; Column 3: Measured Balmer decrement; Columns 4-8: Measured flux of di erent emission lines relative to  $H\beta$ =100, S/N is mentioned in brackets; Column 9: Source of publicly available flux and wavelength calibrated 1D JWST/NIRSPEC grating spectra;

mentioned in brackets; Column 9: Source of publicly available flux and wavelength calibrated 1D JWST Column 10: Reference for first determination of O abundance and source for other line-fluxes of interest Identified from broad H lines as AGN host by Harikane et al. (2023).

<sup>b</sup>Mikulski Archive for Space Telescopes (https://mast.stsci.edu).

<sup>c</sup>CEERS DR07 is available at https://ceers.github.io/dr07.html.

are listed in Table 1 for these nine galaxies, along with the literature sources where their  $[OIII]\lambda$  4363 Å flux and O abundance were first published and where other relevant line flux measurements are also available. The reliability of the flux calibration and its e ect on the determined O and Ar abundances are discussed further in Appendix A. Two of these galaxies (GLASS 150029 and CEERS 1665), having relatively broad H lines, have been reported as AGN hosts by Harikane et al. (2023) while the other seven are SFGs.

We further include four additional high-redshift SFGs in our sample whose relevant line flux measurements, including ionised O and Ar lines, are published in the literature, though their spectra were not available publicly. Two of these SFGs had their O and Ar abundances determined directly based on their [OIII] $\lambda$  4363 Å line detection (Rogers et al. 2024; Welch et al. 2024). For two SFGs at z~2.2, their direct determination of O abundances were based on Keck/MOSFIRE spectra but with temperature sensitive [OII] $\lambda\lambda$  7322,7332 Å line detections, where [ArIII]  $\lambda$  7136 Å line fluxes were also reported (Sanders et al. 2023). We use the published line-flux measurements for these four additional SFGs to determine their O & Ar abundances.

### 2.2. Line- ux measurement

For the galaxies where we had publicly available flux and wavelength calibrated 1D JWST/NIRSPEC grating spectra, the fluxes for the relevant emission-lines were measured using the automated line fitting algorithm, ALFA (Wesson 2016), using their published redshift as an input parameter. After subtracting a globally fitted continuum, ALFA derives fluxes by optimizing the parameters of Gaussian fits to the line profiles using a genetic algorithm; line-blending are also taken into account (see Appendix B). The publicly available spectra of the nine galaxies showing the [OIII]  $\lambda$  4363 Å lines and the ionised Ar lines (either [ArIII]  $\lambda$  7136 Å and/or[ArIV]  $\lambda\lambda$  4711,4740 Å) are shown in Figure 1. Note that for ERO 10612 (z = 7.66), the [ArIII]  $\lambda$  7136 AA line lies beyond the red wavelength limit of NIR-SPEC.

We used stacking techniques to increase the S/N of the observed spectra confirming the identification of the [OIII]  $\lambda$  4363 Å and [ArIII]  $\lambda$  7136 lines (Arnaboldi et al. 2002). Appendix A provides further detailed informa-

As the AGN is unresolved for the two sources, it remains unclear if it is responsible for all their emission-line fluxes. We thus include them in our abundance determination analysis assuming a star-forming ionising source but conservatively they are not considered for the ensuing interpretation.

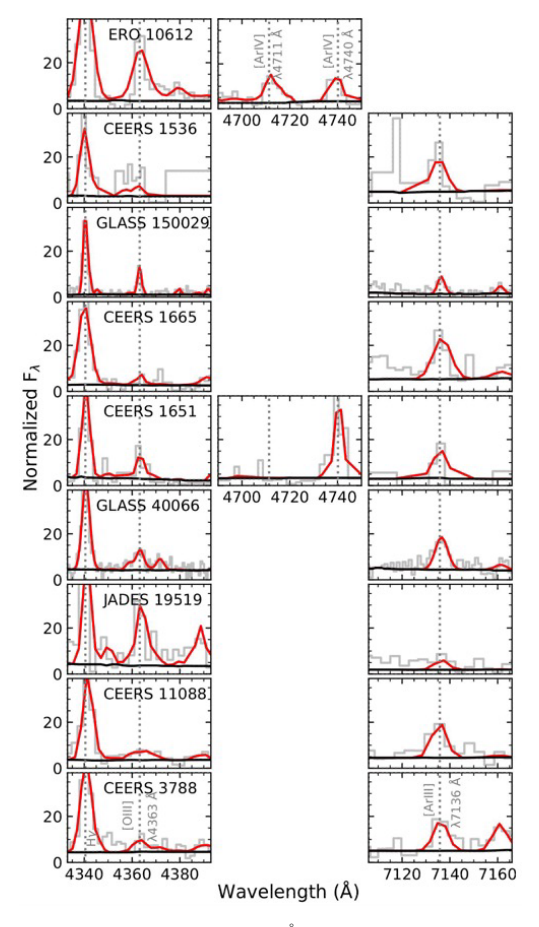


Figure 1 The [OIII]  $\lambda$  4363 Å and detected ionised Ar lines ([ArIV]  $\lambda$  4711 Å, [ArIV]  $\lambda$  4740 Å or [ArIII]  $\lambda$  7136 Å) from the flux and wavelength calibrated publicly-available 1D JWST/NIRSPEC spectra of nine galaxies studied here. The observed spectra is shown in grey while the best-fit spectra is shown in red. The fitted continuum is shown in black.

tion. For each source, the flux ratios of these lines with respect to H $\beta$ , along with their S/N, are noted in Table 1. All other lines of interest, not listed in Table 1, are significantly brighter than [OIII]  $\lambda$  4363 Å line and have been published previously (with almost no measured difference) in the references listed in the same table.

### 2.3. Abundance determination

For each galaxy in our sample, the emission-line fluxes, whether taken from published sources or measured from publicly available spectra, are then passed to NEAT (Nebular Empirical Analysis Tool; Wesson et al. 2012), which applies an empirical scheme to calculate the extinction and elemental abundances. NEAT calculates the intrinsic  $c(H\beta)$  using the flux-weighted ratios of H /H $\beta$ , H $\gamma$ /H $\beta$  and H $\delta$ /H $\beta$  (whichever pairs are observed) and the extinction law of Cardelli et al. (1989), first assuming a nebular temperature of 10000K and an electron density of 1000 cm  $^3$ , and then recalculating  $c(H\beta)$  at the measured temperature and density.

Emission lines fluxes for each galaxy are de-reddened using the calculated  $c(H\beta)$ , see Table 1, and their temperatures and densities are calculated using an iterative process from the relevant diagnostic lines using NEAT (see Wesson et al. 2012, section 3.3). For our observations, NEAT utilizes the temperature-sensitive [OIII] $\lambda$ 4363 Å line, or the  $[OII]\lambda\lambda$  7322,7332 Å lines for the two Keck/MOSFIRE observed galaxies, and the densitysensitive [OII]  $\lambda\lambda$  3726,3729 Å  $\,$  and [SII]  $\lambda\lambda$  6717,6731  $\,$ Å doublets to obtain temperature and electron density for each galaxy spectra. O and Ar ionic abundances are measured from the observed fluxes of the O ([OII]  $\lambda\lambda$  3726,3729 Å , [OIII]  $\lambda\lambda$  4363,4959,5007 Å) and Ar ([ArIII]  $\lambda$  7136 Å and/or [ArIV]  $\lambda\lambda$  4711,4740 Å) lines respectively. ICF correction for O is negligible when lines pertaining to both  $O^{2+}$  (i.e, [OIII]  $\lambda\lambda\lambda$ 5007, 4959, 4363 Å) and O<sup>+</sup> ([OII]  $\lambda\lambda$  3727, 3729 Å) are observed. Elemental Ar abundances are obtained from the ionic abundances utilising the latest ionisation correction factors (ICF; Amayo et al. 2021) for Ar abundance measurement. The impact of the assumed ICF on the determined Ar abundances and thereby the implications for our results are discussed in Appendix C. Uncertainties are propagated through all steps of the analysis into the final values. The galaxy stellar masses, specific-star-formation rates (sSFR) and star-formation timescales (t<sub>SF</sub>) are discussed in Appendix D, and these along with the O and Ar abundances are presented in Table 2.

# 2.4. Comparison with published abundance determinations

In Figure 2 we show that our O abundances, determined following a uniform methodology, are consistent within error with previously published values. Our newly determined  $12 + \log({\rm O/H})$  values have a mean o set of 0.05 dex and standard deviation of 0.06 dex compared to the literature values, well within the errors for individual determinations. We report in this work the first determination of Ar abundances and thereby  $\log({\rm O/Ar})$  for all these galaxies, except for

Table 2 Physical parameters and abundances of galaxies with z=1.3-7.7 studied in this work.

Name	$\mathbf{z}$	$\log(\rm M_*/\rm M_{\odot})$	log(sSFR) [yr <sup>1</sup> ]	t <sub>SF</sub> [Myr]	12 + log(O/H)	$12 + \log(Ar/H)$	log(O/Ar)
ERO 10612	7.66	$7.78 \pm 0.29$	$6.64 \pm 0.29$	$4.37_{2\ 13}^{4\ 13}$	$7.66 \pm 0.1$	$5.82 \pm 0.16$	$1.85 \pm 0.19$
CEERS 1536	5.038	$8.85 \pm 1.09$	$7.65 \pm 1.11$	$44.67_{41}^{53}$ $_{2}^{77}$	$7.51 \pm 0.13$	$5.43 \pm 0.13$	$2.08 \pm 0.18$
GLASS $150029^a$	4.584	$9.12 \pm 0.33$	$8.08 \pm 0.33$	$120.23_{63.99}^{136.81}$	$7.57 \pm 0.05$	$5.35 \pm 0.07$	$2.22 \pm 0.08$
CEERS $1665^a$	4.488	$9.79 \pm 0.92$	$7.37 \pm 0.92$	$23.44_{2}^{171}_{62}^{54}$	$8.24 \pm 0.15$	$5.86 \pm 0.12$	$2.38 \pm 0.18$
CEERS 1651	4.382	$8.85 \pm 0.89$	$7.37 \pm 0.9$	$23.44_{2}^{162}_{49}^{77}$	$7.74 \pm 0.25$	$6.52 \pm 0.26$	$1.22 \pm 0.36$
GLASS 40066	4.02	$9.4 \pm 0.31$	$7.83 \pm 0.31$	$67.61_{34}^{7}_{5}^{43}$	$7.76 \pm 0.17$	$5.53 \pm 0.17$	$2.22\pm0.24$
JADES 19519	3.604	$8.64 \pm 0.1$	$8.04 \pm 0.14$	$109.65_{3}^{41}_{21}^{71}$	$7.36 \pm 0.16$	$5.24 \pm 0.16$	$2.12 \pm 0.23$
CEERS 11088	3.302	9.68	7.35	22.39	$8.16 \pm 0.1$	$5.7 \pm 0.13$	$2.46 \pm 0.16$
$Q2343-D40^{b}$	2.963	-	-	-	$8.09 \pm 0.07^{b}$	$5.45 \pm 0.06^{b}$	$2.64 \pm 0.1^{b}$
CEERS 3788	2.295	9.45	8.82	660.69	$8.15 \pm 0.1$	$5.95 \pm 0.11$	$2.2 \pm 0.14$
COSMOS $19985^b$	2.188	$10.12 \pm 0.04$	$7.8 \pm 0.06$	$63.1_{8}^{9}_{14}^{35}$	$7.89 \pm 0.2^{b}$	$5.33 \pm 0.24^{b}$	$2.58 \pm 0.31^{b}$
COSMOS $20062^b$	2.185	$10.1 \pm 0.07$	$7.68 \pm 0.08$	$47.86_{8}^{9} {}_{5}^{68}$	$8.24 \pm 0.27^{b}$	$5.58 \pm 0.31^{b}$	$2.66 \pm 0.41^{b}$
$SGAS1723+34^b$	1.329	$8.77 \pm 0.15$	$7.88 \pm 0.16$	$75.86_{23}^{33}_{28}^{79}$	$8.13 \pm 0.03^{b}$	$5.69 \pm 0.06^{b}$	$2.43 \pm 0.08^{b}$

Note—Column 1: Name of galaxy; Column 2: galaxy redshift; Column 3-5: Estimated mass, sSFR, and star-formation timescale of galaxies, from their SED tted to broad-band photometry (see Appendix D); Columns 6-8: Estimated elemental abundances. "Identi ed from broad H lines as AGN host by Harikane et al. (2023).

 $<sup>^</sup>b$ For these galaxies, the JWST/NIRSPEC spectra were not available publicly. The abundances were estimated from line fluxes published in the literature.

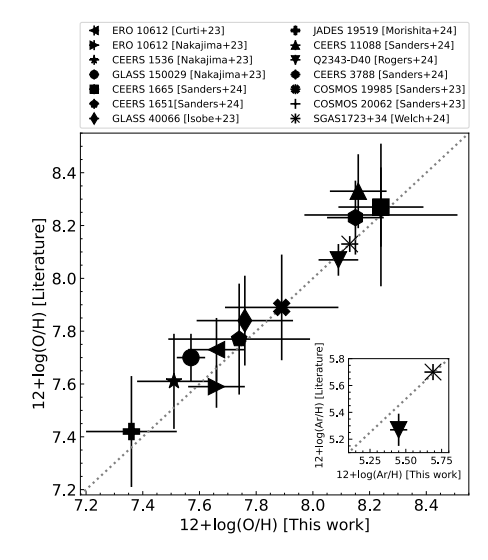


Figure 2  $12 + \log(O/H)$  abundances determined in this work compared to previously published values. The inset shows the same for the two sources with previously published  $12 + \log(Ar/H)$  determinations.

SGAS1723+34 and Q2343-D40. For Q2343-D40, Rogers et al. (2024) reported an Ar abundance slightly lower than our determination, a potential consequence of their choice for a di erent ICF scheme (Izotov et al. 2006) than the one utilised in this work, or arising from di erences in their abundance determination methodology. For SGAS1723+34, Welch et al. (2024) report an Ar

abundance nearly identical to our determination (see Figure 2 [inset]).

# 3. GALAXY CHEMICAL ENRICHMENT AT $$\rm Z{\sim}1.3{\text{--}}7.7$

Figure 3a shows the position of the galaxies at  $z\sim1.3-7.7$  in the  $\log(O/Ar)$  vs  $12 + \log(Ar/H)$  plane, and represents their state of chemical enrichment.

### 3.1. Sources at z~1.3-3.4

Six SFGs (z~1.3-3.4; see Figure 3a) are consistent within error with the Milky Way (MW) solar neighbourhood Galactic Chemical Evolution (GCE) model (Kobayashi et al. 2020a), where CCSNe (including hypernovae) and SNe Ia dominate. Additionally, their position is consistent with the locus traced by the mean log(O/Ar) as a function of 12+log(Ar/H) for the higher mass (M>  $10^9~{\rm M}_{\odot}$ ) low-redshift (z< 0.3) starbursts (log(sSFR)> 8) from SDSS (Brinchmann et al. 2004, Bhattacharya et al. in prep). This remarkably shows that, just like the MW ISM (Matteucci 2021; Kobayashi et al. 2020a) and higher-mass starbursts at z< 0.3, the SFGs in our sample out to z~3.4 are consistent with having chemical enrichment being driven mainly by CCSNe and SNe Ia, with the same nucleosynthesis yields and initial mass functions.

The only other SFG (KBSS-LM1, z=2.396, Steidel et al. 2016) with direct auroral-line measurements

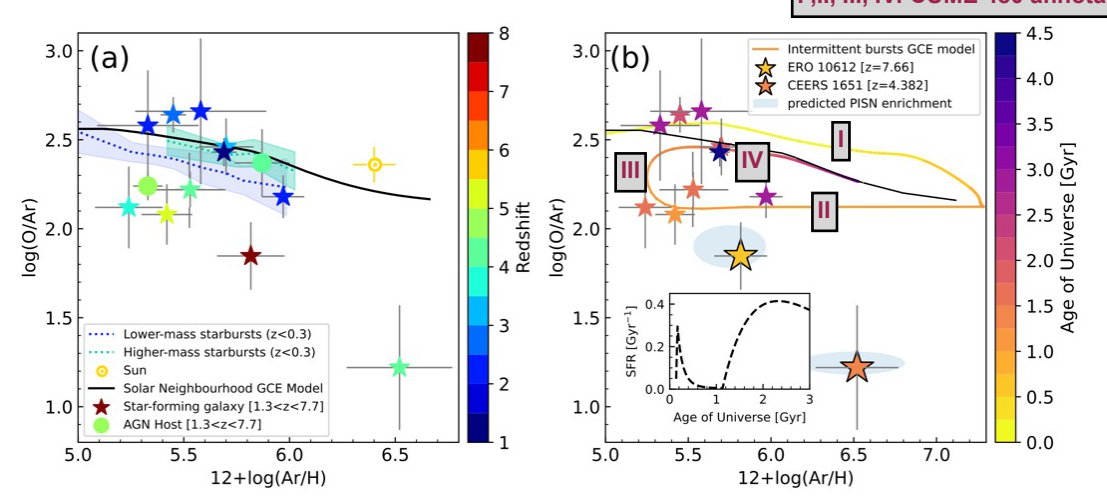


Figure 3 (a) For the nine SFGs and two AGN hosts at  $z\sim1.3$ –7.7,  $\log(O/Ar)$  vs  $12 + \log(Ar/H)$  is shown. The galaxies are coloured by their redshift. The dotted blue and green lines respectively show the sequence of mean values of low-redshift (z<0.3) relatively lower mass ( $M<10^8$  M ) and relatively higher mass ( $M>10^9$  M ) starburst ( $\log(sSFR)>8$ ) galaxies from SDSS (Bhattacharya et al. in prep). Their standard deviations are shaded. The SFGs at  $z\sim1.3$ –3.4 as well as the higher mass low-redshift starbursts are consistent with the Milky Way Solar Neighbourhood GCE model (Kobayashi et al. 2020a) track (black line). (b) Same as panel (a) but now the SFGs are coloured by the age of the universe at their redshift. The plotted GCE models are the same Solar Neighbourhood model (black line), and one for an intermittent starburst scenario, that follows the star-formation history shown in the inset, coloured by age of the universe. The two most  $\log(O/Ar)$ -poor galaxies are highlighted. The  $\log(O/Ar)$  from predicted PISN enrichment yields (Takahashi et al. 2018) corresponding to the observed O abundances of these two galaxies are also marked.

and full-spectral UV-fitting<sup>2</sup> has  $[O/Fe] \sim 0.6 \pm 0.13$  at  $[Fe/H] \sim 1.6$ . This is coincident with the MW solar neighbourhood GCE model in the [O/Fe] vs [Fe/H] plane (see Fig 3 in Kobayashi et al. 2020a), and in extension consistent with the  $z \sim 1.3-3.4$  SFGs presented in this work. This shows, at least for some of our small sample of galaxies, that MW-like chemical enrichment sequences and their underlying mechanisms hold up to  $z \sim 1.3-3.4$ .

#### 3.2. Sources at $z \sim 3.6$ –7.7

Five SFGs (z $\sim$ 3.6–7.7) have log(O/Ar) values below even the sequence traced by lower-mass (M<  $10^8~M_{\odot}$ ) z< 0.3 starbursts (Figure 3a). The Ar abundance may be underestimated if a large fraction of Ar is condensed in dust grains but given that O and Ar have similar dust condensation temperatures (Savage & Sembach 1996), it is unlikely that the lower log(O/Ar) for these SFGs is

caused by more O being ejected with dust grains than Ar. This implies that the  $z{\sim}3.6{\text -}7.7$  SFGs are characterised by unusually high Ar production, relative to O. In the following subsections, we discuss possible scenarios that may be responsible for the low  $\log({\rm O/Ar})$  values for these galaxies.

# 3.3. Potential chemical enrichment from intermittent starbursts at z~3.6−7.7

Keeping the same assumption of the chemical enrichment recipe for the solar neighbourhood (Kobayashi et al. 2020a), we construct a tailored GCE model considering two bursts of star-formation at very early times (with substantial infall of pristine gas between the bursts), to try and explain the position of the z $\sim$ 3.6–7.7 SFGs in this plane (see Figure 3b). An intermittent star-formation model has previously been invoked to explain measurements of emission line fluxes in similar high redshift SFGs (Kobayashi & Ferrara 2024). Note that the purpose of constructing this specific model is to check if the low  $\log(\mathrm{O/Ar})$  values of these galaxies may be explained by considering an extreme star-formation history but keeping the MW-like CCSNe and SNe Ia dominated nucleosynthesis.

Other SFGs with [Fe/H] determined from full-spectral UV-fitting (e.g. Cullen et al. 2019, 2021; Stanton et al. 2024) have [O/H] (in lieu of abundance) determined from strong-line methods from optical emission-lines, which may be over-estimated if not calibrated against direct methods (Maiolino & Mannucci 2019).

In Figure 3b (inset), the star-formation history of the GCE model is plotted. An initial burst of star formation at the break of cosmic dawn is followed by a quiescent phase up to  $\sim 1.1$  Gyr after the birth of the universe, when the ISM is enriched through continued explosions of Type Ia SNe to very high 12 + log(Ar/H) values and minimum log(O/Ar) values (Figure 3b). This is followed by an infall of primordial gas that strongly dilutes the ISM, reducing  $12 + \log(Ar/H)$  keeping  $\log(O/Ar)$ constant, and induces another episode of star-formation that starts re-enriching the ISM (Figure 3b inset). Thus a loop in the  $\log(O/Ar)$  vs  $12 + \log(Ar/H)$  plane is formed which is a signature of gas infall (Spitoni et al. 2019; Arnaboldi et al. 2022; Kobayashi et al. 2023). Other models with less extreme star-formation histories (lower star formation rates with continuous or intermittent star-formation with and without gas infall) will occupy the parameter space within the loop spanned by this extreme model in this plane.

The model can successfully explain the positions of three of the z $\sim$ 3.6–7.7 SFGs that have log(O/Ar) $\sim$ 2.1. However, two of our SFGs that have log(O/Ar) values  $3\sigma$  lower than the MW solar neighbourhood GCE model (highlighted in Figure 3b) are also below the log(O/Ar) values reached by this model. These two galaxies are ERO 10612, which is the highest redshift galaxy in our sample at z=7.66, i.e, just 672 Myr after the birth of the universe, and CEERS 1651 at z=4.382 (1.37 Gyr after the birth of the universe). It is unclear whether CC-SNe and SNe Ia dominated chemical enrichment models could explain these low-log(O/Ar) galaxies.

# 3.4. Additional potential sources of chemical enrichment at z~3.6−7.7

A potential mechanism for  $\log(O/Ar)$ -poor stellar populations would be to assume a higher SNIa rate (e.g. with a higher binary fraction) relative to CCSNe for a given stellar population mass in the early universe, than is seen for the MW solar neighbourhood.

Another potential mechanism for Ar enhancement would be the inclusion of sub-Chandrasekhar mass SNe Ia (sub-Ch SNe Ia; see Kobayashi et al. 2020b and references therein) in the GCE models. These sub-Ch SNe Ia have been suggested to be the main enrichment source for observed MW dwarf spheroidal satellite galaxies, which formed their masses at early times and have been quiescent since (Kirby et al. 2019). GCE models including sub-Ch SNe Ia (Kobayashi et al. 2020b) predict very low  $\log({\rm O/Ar})$ , as well as low [ /Fe], because of the higher occurrence of sub-Ch SNe Ia relative to Ch-mass SNe Ia at early times (after  $\sim 40~{\rm Myr}$ ).

Another potential rapid metal enrichment source is pair-instability supernovae (PISNe; Heger & Woosley 2002; Nomoto et al. 2013) that have been predicted to evolve from massive (> 140  $M_{\odot}$ ) population III stars<sup>3</sup> having only  $\sim 2$  Myr (Takahashi et al. 2018) lifespans. Their metal contribution to the ISM is expected to be visible only for a short time after the first generation of stars formed (Hartwig et al. 2018; Vanni et al. 2023), to be washed-out rapidly (Ji et al. 2015) once CCSNe enrichment processes begin after  $\sim 20~{\rm Myr}$  (Kobayashi et al. 2020a). Given the small, albeit uncertain, t<sub>SF</sub> values (see Table 2) for ERO 10612 and CEERS 1651, PISNe may potentially be responsible for their observed Ar enhancement, but only if there has been no mixing with any pre-enriched ISM or mass-loss from preexisting stars. From stellar nucleosynthesis vields of PISNe (Takahashi et al. 2018), the log(O/Ar) values of ERO 10612 and CEERS 1651 (see Figure 3b) are consistent with that expected from lower-mass (170-180 M<sub>☉</sub>) and higher-mass (260-280  $M_{\odot}$ ) PISN progenitors respectively<sup>4</sup>. However, in GCE models with reasonable assumptions, the PISN enrichment causes the rapid decrease of log(O/Ar) to very low values at much lower metallicities (Kobayashi et al. in prep).

#### 4. SUMMARY AND CONCLUSIONS

We extend the use of the  $\log({\rm O/Ar})$  vs  $12 + \log({\rm Ar/H})$  plane (Arnaboldi et al. 2022; Kobayashi et al. 2023) for inferring the mechanisms that govern galaxy chemical enrichment to SFGs, o ering a direct analogy to the [ /Fe] vs [Fe/H] plane for stars. We robustly obtain line-flux measurements for 7 SFGs from their flux and wavelength calibrated 1D JWST/NIRSPEC spectra (see Table 1), in addition to 4 SFGs where such flux measurements were available from their literature sources (see Section 2). We then directly determine O and Ar abundances for these 11 SFGs at z $\sim$ 1.3–7.7 from observations of temperature sensitive auroral lines (Table 2).

We present their positions in the  $\log({\rm O/Ar})$  vs 12 +  $\log({\rm Ar/H})$  plane (Figure 3a). Six SFGs (z $\sim$ 1.3–3.4) are consistent within error with a MW-like CCSNe and SNe Ia dominated chemical enrichment model (Kobayashi et al. 2020a). Thus at least for some of our small sample of galaxies, MW-like chemical enrichment sequences and their underlying mechanisms are in place as early as z $\sim$ 1.3–3.4.

 $<sup>^3</sup>$  First generation metal-free stars formed from pristine gas.

<sup>&</sup>lt;sup>4</sup> Computed assuming the observed O abundances of these two SFGs (see Table 2) and the log(O/Ar) values for non-rotating PISNe of di erent progenitor masses in Takahashi et al. (2018, see their Figure 9).

Five SFGs ( $z\sim3.6$ –7.7), however, are  $\log({\rm O/Ar})$ -poor compared to the MW GCE model track (Figure 3a). The  $\log({\rm O/Ar})$  values of three of these may be explained through a tailored GCE model with early intermittent star-formation, but keeping the MW-like CCSNe and SNe Ia dominated chemical enrichment (see Section 3.3). For the other two, ERO 10612 and CEERS 1651, additional potential sources of chemical enrichment may be required. Tailored GCE models will be utilised to better understand the rapid enrichment of these SFGs (Kobayashi et al. in prep).

The ever-improving quality of JWST/NIRSPEC data and upcoming large ground-based spectroscopic surveys (e.g. the Prime Focus Spectrograph galaxy evolution survey at Subaru; Greene et al. 2022), implies that it should be possible to build-up a large sample of SFGs with direct determinations of O and Ar abundances from auroral line-flux measurements. In conjunction with tailored GCE models, such a large sample of galaxies with elemental abundance determinations will enable further refinement in the understanding of galaxy chemical enrichment mechanisms presented in this work. There is, thus, now a new window for constraining galaxy chemical enrichment from present day to the early universe.

SB was supported by the INSPIRE Faculty award (DST/INSPIRE/04/2020/002224), Department of Science and Technology (DST), Government of India. SB and MAR acknowledge support to this research from the European Southern Observatory, Garching, through the 2022 SSDF. SB and OG acknowledge support to this research from Excellence Cluster ORIGINS, which is funded by the Deutsche Forschungsgemenschaft (DGF, German Research Foundation) under Germany's Excellence Strategy - EXC-2094-390783311. MAR and OG thank the Research School of Astronomy and Astrophysics at ANU for support through their Distinguished Visitor Program in 2024. This work was supported by the DAAD under the Australia-Germany joint research programme with funds from the Australian Ministry for Science and Education. CK acknowledges funding from the UK Science and Technology Facility Council through grant ST/Y001443/1.

 $Facilities \quad {\rm JWST~(NIRSPEC),~Keck~(MOSFIRE),} \\ {\rm SDSS}$ 

Software AstroPy (Astropy Collaboration et al. 2013), SciPy (Virtanen et al. 2020), NumPy (Oliphant 2015), Matplotlib (Hunter 2007), NEAT (Wesson et al. 2012) and ALFA (Wesson 2016).

## APPENDIX

## A. FLUX CALIBRATION AND LINE DETECTION FROM JWST/NIRSPEC SPECTRA

As the wavelength and flux calibrated spectra were downloaded from public archives, one cannot rule out possible significant di erences of the line-fluxes and abundances determined from them in this work with those previously published (references noted in Table 1). In Figure 2 we show that our determined O abundances are always consistent within error with previously published values, showing negligible o set (0.05 dex) and dispersion (0.06 dex,

see Section 2.4). Our measured [OIII]  $\lambda$  4363 Å line fluxes (see Table 1) are also consistent with their previously published values. The tight correlation between the O abundance values from literature and those determined in this work implies that the flux calibration in the spectra range  $\sim$ 3700–6750 Å is robust and consistent between the spectra used here and those utilised previously. Since the [ArIII]  $\lambda$  7136 Å line is sufficiently close to the redder limit of the aforementioned wavelength range, the flux calibration properties apply also to this line.

We carried out additional tests to verify the reliable detections of the [OIII]  $\lambda$  4363 Å and [ArIII]  $\lambda$  7136 Å line line fluxes in the publicly available JWST/NIRSPEC spectra. If the observed rest-frame 1D spectra (normalised to a given line flux) are stacked, the S/N of a detected line should show an increase of an order of the square root of the number of spectra being stacked, in case of poissonian noise (e.g. Arnaboldi et al. 2002). We make two stacked SFG spectra with the flux and wavelength calibrated 1D JWST spectra (each normalised to H $\beta$  flux), one for z< 3.4 with CEERS 11088 and 3788 (as we do not have the publicly available spectra for other SFGs at these redshifts; see Table 2), and another for z> 3.6 with CEERS 1536 and 1651, GLASS 40066 and JADES 19519 (as only these four are SFGs that have the [ArIII]  $\lambda$  7136 Å line). For the z< 3.4 stack, we find that the [OIII]  $\lambda$  4363 Å and [ArIII]  $\lambda$  7136 Å lines are detected with S/N of 5.97 and 7.3 respectively, showing the expected increase in S/N compared to the line detection in individual spectra. For the z> 3.6 stack, we find that the [OIII]  $\lambda$  4363 Å and [ArIII]  $\lambda$  7136 Å lines are detected with S/N of 7.66 and 9.73 respectively, also showing the expected S/N increase compared to the detection in individual spectra.

We additionally note that the CEERS 11088 galaxy was observed with the [ArIII]  $\lambda$  7136 Å line detected in two separate JWST/NIRSPEC grism observations (G235M/F170LP and G395M/F290LP) as it occurs in the overlapping wavelength region. The [ArIII] line is detected with S/N> 6 in both spectra from di erent grism observations, with similar line flux values within error, as reported in Table 1. The independent line detection and concordance of measured fluxes additionally certifies the [ArIII]  $\lambda$  7136 Å line detection for this galaxy but also attests to the reliable flux calibration for those galaxies with CEERS DR07 spectra (see Table 1). Note also that while we use the flux and wavelength calibrated 1D spectra from the source reported in Table 1, we have also checked other sources when available, such as the DAWN JWST archive (https://dawn-cph.github.io/dja/) that employ di erent flux and wavelength calibrations. While there may be minor discrepancy in the measured fluxes of individual lines when comparing the calibrated 1D spectra of a galaxy from di erent public sources, we find that, for the galaxies in our sample, the determined O and Ar abundances are always consistent within error.

#### B. IMPACT OF LINE-BLENDING ON AR ABUNDANCES

The majority of the O and Ar lines used in this work are not expected to be blended with other lines. Only the  $[ArIV]\lambda$  4711 Å line, seen only for ERO 10612 in our sample, may occasionally be blended with the HeI  $\lambda$  4713 Å line. The genetic fitting algorithm of ALFA fits the observed spectra simultaneously to a number of lines, including the  $[ArIV]\lambda$  4711 Å and HeI  $\lambda$  4713 Å lines. Given the spectral resolution and the observed flux distribution  $\sim$ 4711 Å for ERO 10612, any observed flux was determined by ALFA to be attributed solely to  $[ArIV]\lambda$  4711 Å, with no contribution from the HeI  $\lambda$  4713 Å line (if both lines had contributed to the observed flux, then the flux distribution would have been broader). We note that even if these two lines are blended, and the determined Ar abundance of ERO 10612 is overestimated, any potential correction will result in reducing the Ar abundance while increasing its  $\log(O/Ar)$  by the same value, thereby still keeping the same diagonal o set in Figure 3 from the MW-like chemical enrichment sequence in the  $\log(O/Ar)$  vs 12 +  $\log(Ar/H)$  plane.

## C. IMPACT OF IONISATION CORRECTION FACTORS ON AR ABUNDANCES

For Ar, the ionisation states of  $Ar^{2+}$ ,  $Ar^{3+}$ , and in smaller amounts  $Ar^+$  and  $Ar^{4+}$  are possible for an SFG. Hence the ICF correction to the observed ionic abundances is relevant for Ar abundance determination. Arellano-Córdova et al. (2024) found that di erent ICF schemes, including Amayo et al. (2021) used here, have worked equally well for Ar abundance determination. They found that for  $z\sim0.1$  SFGs with  $12 + \log(O/H) > 8.2$ , ICF correction from observing only [ArIII]  $\lambda$  7136 Å may underestimate the Ar abundance by up to  $\sim 0.4$  dex in their sample, but no such e ect is seen when  $12 + \log(O/H) < 8.2$ . This implies that the resulting  $\log(O/Ar)$  values would be higher than their actual intrinsic values. The ICF correction based on the observation of both [ArIII] and [ArIV] lines is more accurate instead at all  $12 + \log(O/H)$  values (see their Figure 3). Only one of our SFGs (COSMOS 20062) has  $12 + \log(O/H) > 8.2$  with its Ar abundance value determined from the observed  $Ar^{2+}$  lines only. Its Ar abundance value may indeed be underestimated but even considering the maximum o set, its  $\log(O/Ar)$  abundance would still be consistent

with MW-like chemical enrichment, as it is the galaxy with the highest  $\log(O/Ar)$  in our sample (see Table 2). Other SFGs in our sample have  $12 + \log(O/H) < 8.2$  and thus no ICF correction bias is expected.

# D. STELLAR MASS, SPECIFIC-STAR-FORMATION-RATE AND STAR-FORMATION-TIMESCALES OF THE GALAXY SAMPLE

For all the galaxies with z>4, the stellar mass and sSFR (noted in Table 2) were reported by Nakajima et al. (2023), based on their JWST Spectral Energy Distribution (SED) fitting with assumed initial mass function (IMF) from Chabrier (2003). For JADES 19519, the stellar mass and sSFR based on JWST SEDs was reported by Morishita et al. (2024). For CEERS 11088 and 3788, we instead report the Hubble Space Telescope SED- based (Momcheva et al. 2016) estimates of stellar mass and sSFR with the same assumed IMF. The stellar mass and sSFR for COSMOS 19985 and 20062 (Sanders et al. 2023) and SGAS1723+34 (Florian et al. 2021) are also noted in Table 2 but these estimates are not available for Q2343-D40. Star-formation timescale is computed with the simple approximation of  $t_{\rm SF}=1/{\rm sSFR}$ . We note that a top-heavy IMF would reduce the stellar masses of the galaxies by  $\sim 0.5$  dex (Harvey et al. 2024).

#### REFERENCES

Amayo, A., Delgado-Inglada, G., & Stasińska, G. 2021, MNRAS, 505, 2361, doi: 10.1093/mnras/stab1467
Arellano-Córdova, K. Z., Berg, D. A., Mingozzi, M., et al. 2024, ApJ, 968, 98, doi: 10.3847/1538-4357/ad34cf
Arnaboldi, M., Aguerri, J. A. L., Napolitano, N. R., et al. 2002, AJ, 123, 760, doi: 10.1086/338313

Arnaboldi, M., Bhattacharya, S., Gerhard, O., et al. 2022, A&A, 666, A109, doi: 10.1051/0004-6361/202244258

Astropy Collaboration, Robitaille, T. P., Tollerud, E. J., et al. 2013, A&A, 558, A33, doi: 10.1051/0004-6361/201322068

Beverage, A. G., Kriek, M., Suess, K. A., et al. 2024a, ApJ, 966, 234, doi: 10.3847/1538-4357/ad372d

Beverage, A. G., Slob, M., Kriek, M., et al. 2024b, arXiv e-prints, arXiv:2407.02556, doi: 10.48550/arXiv.2407.02556

Bhattacharya, S., Arnaboldi, M., Gerhard, O., et al. 2021, A&A, 647, A130, doi: 10.1051/0004-6361/202038366

Bhattacharya, S., Arnaboldi, M., Hartke, J., et al. 2019, A&A, 624, A132, doi: 10.1051/0004-6361/201834579

Bhattacharya, S., Arnaboldi, M., Caldwell, N., et al. 2022, MNRAS, 517, 2343, doi: 10.1093/mnras/stac2703

Brinchmann, J., Charlot, S., White, S. D. M., et al. 2004, MNRAS, 351, 1151,

doi: 10.1111/j.1365-2966.2004.07881.x

Bunker, A. J., Cameron, A. J., Curtis-Lake, E., et al. 2023, arXiv e-prints, arXiv:2306.02467,

doi: 10.48550/arXiv.2306.02467

Cardelli, J. A., Clayton, G. C., & Mathis, J. S. 1989, ApJ, 345, 245, doi: 10.1086/167900

Chabrier, G. 2003, PASP, 115, 763, doi: 10.1086/376392
 Cullen, F., McLure, R. J., Dunlop, J. S., et al. 2019,
 MNRAS, 487, 2038, doi: 10.1093/mnras/stz1402

Cullen, F., Shapley, A. E., McLure, R. J., et al. 2021, MNRAS, 505, 903, doi: 10.1093/mnras/stab1340

Curti, M., D'Eugenio, F., Carniani, S., et al. 2023, MNRAS, 518, 425, doi: 10.1093/mnras/stac2737

Edvardsson, B., Andersen, J., Gustafsson, B., et al. 1993, A&A, 275, 101

Esteban, C., Bresolin, F., García-Rojas, J., & Toribio San Cipriano, L. 2020, MNRAS, 491, 2137, doi: 10.1093/mnras/stz3134

Florian, M. K., Rigby, J. R., Acharyya, A., et al. 2021, ApJ, 916, 50, doi: 10.3847/1538-4357/ac0257

Fuhrmann, K. 1998, A&A, 338, 161

Greene, J., Bezanson, R., Ouchi, M., Silverman, J., & the PFS Galaxy Evolution Working Group. 2022, arXiv e-prints, arXiv:2206.14908, doi: 10.48550/arXiv.2206.14908

Greene, J. E., Murphy, J. D., Graves, G. J., et al. 2013,  $\label{eq:ApJ} ApJ, 776, 64, \ doi: \ 10.1088/0004\text{-}637X/776/2/64$ 

Harikane, Y., Zhang, Y., Nakajima, K., et al. 2023, ApJ, 959, 39, doi: 10.3847/1538-4357/ad029e

Hartwig, T., Yoshida, N., Magg, M., et al. 2018, MNRAS, 478, 1795, doi: 10.1093/mnras/sty1176

Harvey, T., Conselice, C., Adams, N. J., et al. 2024, arXiv e-prints, arXiv:2403.03908,

 ${\bf doi\colon 10.48550/arXiv.2403.03908}$ 

Hayden, M. R., Bovy, J., Holtzman, J. A., et al. 2015, ApJ, 808, 132, doi: 10.1088/0004-637X/808/2/132

Heger, A., & Woosley, S. E. 2002, ApJ, 567, 532, doi: 10.1086/338487

Hunter, J. D. 2007, Computing In Science & Engineering, 9, 90, doi: 10.1109/MCSE.2007.55

Isobe, Y., Ouchi, M., Tominaga, N., et al. 2023, ApJ, 959, 100, doi: 10.3847/1538-4357/ad09be

- Izotov, Y. I., Stasińska, G., Meynet, G., Guseva, N. G., & Thuan, T. X. 2006, A&A, 448, 955,  ${\bf doi:\ } 10.1051/0004\hbox{-}6361\hbox{:}20053763$
- Jakobsen, P., Ferruit, P., Alves de Oliveira, C., et al. 2022,  $A\&A,\,661,\,A80,\,\mathrm{doi}\colon 10.1051/0004\text{-}6361/202142663$
- Ji, A. P., Frebel, A., & Bromm, V. 2015, MNRAS, 454, 659, doi: 10.1093/mnras/stv2052
- Kirby, E. N., Xie, J. L., Guo, R., et al. 2019, ApJ, 881, 45, doi: 10.3847/1538-4357/ab2c02
- Kobayashi, C., Bhattacharya, S., Arnaboldi, M., & Gerhard, O. 2023, ApJL, 956, L14, doi: 10.3847/2041-8213/acf7c7
- Kobayashi, C., & Ferrara, A. 2024, ApJL, 962, L6, doi: 10.3847/2041-8213/ad1de1
- Kobayashi, C., Karakas, A. I., & Lugaro, M. 2020a, ApJ, 900, 179, doi: 10.3847/1538-4357/abae65
- Kobayashi, C., Leung, S.-C., & Nomoto, K. 2020b, ApJ, 895, 138, doi: 10.3847/1538-4357/ab8e44
- Kriek, M., Conroy, C., van Dokkum, P. G., et al. 2016, Nature, 540, 248, doi: 10.1038/nature20570
- Kuntschner, H., Emsellem, E., Bacon, R., et al. 2010,  $MNRAS,\,408,\,97,\,doi:\,10.1111/j.1365\text{--}2966.2010.17161.x}$
- Lonoce, I., Longhetti, M., Maraston, C., et al. 2015, MNRAS, 454, 3912, doi: 10.1093/mnras/stv2150
- Maiolino, R., & Mannucci, F. 2019, A&A Rv, 27, 3, doi: 10.1007/s00159-018-0112-2
- Matteucci, F. 2021, A&A Rv, 29, 5, doi: 10.1007/s00159-021-00133-8
- Momcheva, I. G., Brammer, G. B., van Dokkum, P. G., et al. 2016, ApJS, 225, 27,
- doi: 10.3847/0067-0049/225/2/27
- Morishita, T., Stiavelli, M., Grillo, C., et al. 2024, arXiv e-prints, arXiv:2402.14084, doi: 10.48550/arXiv.2402.14084
- Nakajima, K., Ouchi, M., Isobe, Y., et al. 2023, ApJS, 269, 33, doi: 10.3847/1538-4365/acd556
- Nomoto, K., Kobayashi, C., & Tominaga, N. 2013, ARA&A, 51, 457,
  - doi: 10.1146/annurev-astro-082812-140956
- Oliphant, T. E. 2015, Guide to NumPy, 2nd edn. (USA: CreateSpace Independent Publishing Platform)
- Onodera, M., Carollo, C. M., Renzini, A., et al. 2015, ApJ, 808, 161, doi: 10.1088/0004-637X/808/2/161

- Pagel, B. E. J. 1997, Nucleosynthesis and Chemical Evolution of Galaxies
- Rogers, N. S. J., Strom, A. L., Rudie, G. C., et al. 2024, ApJL, 964, L12, doi: 10.3847/2041-8213/ad2f37
- Sanders, R. L., Shapley, A. E., Topping, M. W., Reddy, N. A., & Brammer, G. B. 2024, ApJ, 962, 24, doi: 10.3847/1538-4357/ad15fc
- Sanders, R. L., Shapley, A. E., Clarke, L., et al. 2023, ApJ, 943, 75, doi: 10.3847/1538-4357/aca9cc
- Sargent, W. L. W. 1970, ApJ, 160, 405, doi: 10.1086/150443
- Savage, B. D., & Sembach, K. R. 1996, ARA&A, 34, 279, doi: 10.1146/annurev.astro.34.1.279
- Spitoni, E., Silva Aguirre, V., Matteucci, F., Calura, F., & Grisoni, V. 2019, A&A, 623, A60, doi: 10.1051/0004-6361/201834188
- Stanton, T. M., Cullen, F., McLure, R. J., et al. 2024, MNRAS, 532, 3102, doi: 10.1093/mnras/stae1705
- Steidel, C. C., Strom, A. L., Pettini, M., et al. 2016, ApJ, 826, 159, doi: 10.3847/0004-637X/826/2/159
- Takahashi, K., Yoshida, T., & Umeda, H. 2018, ApJ, 857, 111, doi: 10.3847/1538-4357/aab95f
- Thomas, D., Maraston, C., Bender, R., & Mendes de Oliveira, C. 2005, ApJ, 621, 673, doi: 10.1086/426932
- Tinsley, B. M. 1980, FCPh, 5, 287, doi: 10.48550/arXiv.2203.02041
- Topping, M. W., Shapley, A. E., Reddy, N. A., et al. 2020, MNRAS, 495, 4430, doi: 10.1093/mnras/staa1410
- Trager, S. C., Faber, S. M., Worthey, G., & González, J. J. 2000, AJ, 119, 1645, doi: 10.1086/301299
- Vanni, I., Salvadori, S., Skúladóttir, Á., Rossi, M., & Koutsouridou, I. 2023, MNRAS, 526, 2620, doi: 10.1093/mnras/stad2910
- Virtanen, P., Gommers, R., Oliphant, T. E., et al. 2020, Nature Methods, 17, 261, doi: 10.1038/s41592-019-0686-2
- Welch, B., Olivier, G. M., Hutchison, T. A., et al. 2024, arXiv e-prints, arXiv:2401.13046, doi: 10.48550/arXiv.2401.13046
- Wesson, R. 2016, MNRAS, 456, 3774,
- doi: 10.1093/mnras/stv2946
- Wesson, R., Stock, D. J., & Scicluna, P. 2012, MNRAS, 422, 3516, doi: 10.1111/j.1365-2966.2012.20863.x